Available online at www.sciencedirect.com

SciVerse ScienceDirect

Russian Geology and Geophysics 54 (2013) 555–565

RUSSIAN GEOLOGY AND GEOPHYSICS

www.elsevier.com/locate/rgg

Permafrost and groundwater settings at the site of "Kraton-3" peaceful underground nuclear explosion (*Yakutia*), from TEM data

S.Yu. Artamonova [a,*], N.O. Kozhevnikov [b], E.Yu. Antonov [b]

[a] *V.S. Sobolev Institute of Geology and Mineralogy, Siberian Branch of the Russian Academy of Sciences, pr. Akademika Koptyuga 3, Novosibirsk, 630090, Russia*

[b] *A.A. Trofimuk Institute of Petroleum Geology and Geophysics, Siberian Branch of the Russian Academy of Sciences, pr. Akademika Koptyuga 3, Novosibirsk, 630090, Russia*

Received 21 March 2012; accepted 14 September 2012

Abstract

Geological and geophysical interpretation of TEM data has revealed changes to the subsurface from the "Kraton-3" peaceful underground nuclear explosion (PUNE). The explosion was conducted on 24 August 1978 at a depth of 577 m in Middle Cambrian limestone on the eastern periphery of the Tunguska basin (Western Yakutia). The site is located in an area of 100 to 300 m thick permafrost and pressurized aquifers with Na-Ca-Cl brines (up to 400 g/l TDS) and cryopegs. The "Kraton-3" epicenter is only 160 m away from a fault emerging along the Markha River.

TEM responses collected at 22 stations along three profiles image a layered-earth background resistivity pattern. The highly resistive uppermost layer, ~150–200 m thick, consists of perennially frozen ice-rich rocks. Dry permafrost on watersheds of the Markha right side reaches 1200 ohm·m, while the hypsometrically lower frozen ground along the fault is 10 to 40 times less resistive. That is exactly the place of the PUNE epicenter, and the resistivity lows may record permafrost degradation and taliks (unfrozen layers).

The layers below are conductive and correspond to Upper Cambrian and Middle Cambrian (I) aquifers with brines. The top of the Upper Cambrian aquifer along the central profile is highly variable in depth, especially along the fault on the river left bank. The data indicate a local groundwater anomaly above the explosion: the Middle Cambrian I brines, which show up as a conductor in the resistivity pattern, become ~300 m shallower, most likely rising along the rubble chimney above the UNE containment cavity; the lateral extent of the anomaly reaches 400 m. There may exist paths for mass and heat transport maintained by pressurized brines in the system "containment cavity–rubble chimney–fault zone–ground surface".

Keywords: peaceful underground nuclear explosion (PUNE); geological–technological system; subsurface; groundwater; permafrost; TEM survey; environment risk; Siberian craton; Tunguska basin

Introduction

Sites of peaceful underground nuclear explosions (PUNE) are complex geological–technological systems with a decades-long history of relaxation after a strong thermal, radiation, and mechanic impact on the surrounding rocks. The containment cavities left by explosions are actually uncontrollable open underground storages of fission products. The state of the subsurface in the PUNE vicinity requires special studies indispensable for predicting and mitigating the related environment risks.

The 22-kt contained nuclear explosion "Kraton-3" was conducted on 24 August 1978, 38 km away from Aikhal Village, on the right side of the Markha River in Western Yakutia. Technological errors in plugging the emplacement hole (the hole where the charge was placed) led to accidental escape of radioactivity (~2%) in the form of a gas-dust cloud, from the hole mouth.

The TEM data are used in this study to model the permafrost and groundwater settings at the "Kraton-3" PUNE site.

Geological background

The explosion site (Fig. 1) is located within the Central Siberian Plateau, in the eastern margin of the Tunguska basin (Siberian craton). It is an area of hilly topography, with watersheds at 400–440 m and river tables at 100–150 m above

* Corresponding author.
E-mail address: artam@igm.nsc.ru (S.Yu. Artamonova)

1068-7971/$ - see front matter © 2013, V.S. Sobolev IGM, Siberian Branch of the RAS. Published by Elsevier B.V. All rights reserved.
http://dx.doi.org/10.1016/j.rgg.2013.04.007

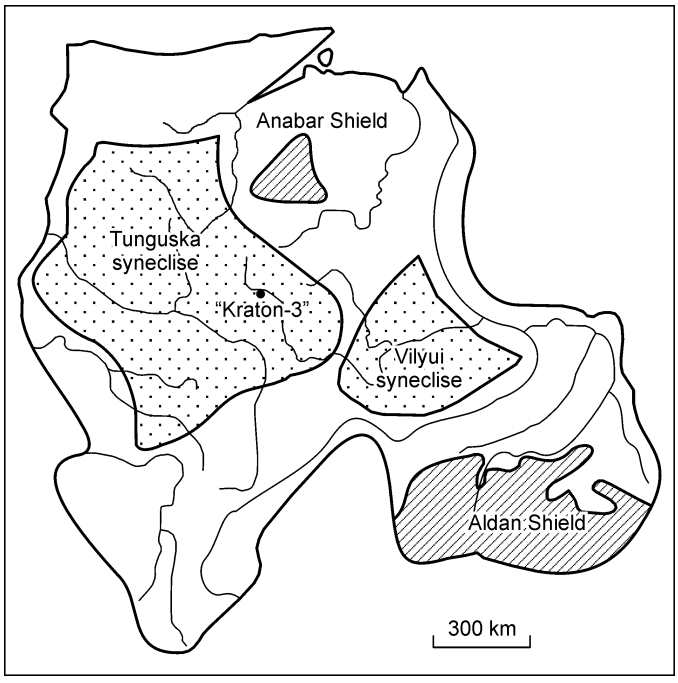

Fig. 1. Location map of "Kraton-3" underground nuclear explosion in Siberian craton.

sealevel (asl). The water table of the Markha River in the PUNE vicinity is about 290 asl.

The local geology (Fig. 2) consists of stratigraphically concordant Lower Ordovician, Cambrian, and Ediacaran sediments, 2400 m of total thickness, lying over an Archean basement (Alekseev, 2009). The sediments are mainly shallow-marine limestones and dolomites, or their clayey and marly varieties, with plane or monoclinal bedding dipping at 10º–12º to the southwest, toward the interior of the paleosea.

The Ediacaran sediments are dolimites and stromatolitic dolomites with marl and sandstone interbeds, 190 m thick in total. Cambrian limestones and dolomites, about 2000 m, constitute the largest portion of the sedimentary section. The upper section consists of 240 m thick Lower Ordovician limestone with mudrock layers lying under Quaternary alluvial loam, pebbles, and debris. The Quaternary deposits are restricted to topographic lows and are as thin as 2 m on watersheds and hill slopes and 10 m in valleys.

The area belongs to the permafrost zone: The upper 100 to 300 m of sediments are perennially frozen and ice-rich (frozen water fills pores, cracks, and vugs). Below there are low-temperature rocks with cryopeg lenses (frozen saline water and brines in voids) and dry frost-bound rocks. The 0 °C isotherm lies at a depth of 800–1050 m (Klimovsky and Gotovtsev, 1994).

The buried aquifers are laterally discontinuous. Their extent correlates with the occurrence of fractured rocks and karst, which are especially abundant along faults.

The interval between +50 and –100 m relative to the sealevel is occupied by variegated clayey limestone and dolomite sediments with rock salt pseudomorphs, as well as separate layers of limestone and dolomite with karst which belong to the Upper Cambrian Markoka Formation (132 m thick). There is a 2–3 to 10–30 m thick undersaturated fractured-porous *Upper Cambrian aquifer* in this depth interval, associated with the Markoka thin fractured clayey limestone and the upper Markha Formation. The water salinity in it varies from 30 to 200 g/l, 90 g/l TDS on average.

The underlying Upper Cambrian Markha Formation consists of clayey, dolomitic, silty, and sandy limestones (Fig. 2). The clayey limestones make the upper confining bed for the *Middle Cambrian aquifer I* of a porous vuggy limestone-dolomite member. The aquifer lies at depths between –300 and –600 m, is 250 m thick on average, and bears 300 g/l sodic-calcium-chloride brines. At the density of saline water ~1.22 g/cm^3 and the pore pressure 4.5–9 mPa (Alekseev, 2009), the pressure head must be 360 to 730 m above the aquifer. The lower confining bed is composed of dense dolomite of the Udachnaya Formation.

The *Middle Cambrian aquifer II* is located mainly within vuggy porous zones of bioherms at depths from 1000 to 1120 m below sealevel, with the pressure head estimated in different ways to be at 310–350 m (Mikulenko et al., 2006) or ~565 m, or locally up to 1270 m (Alekseev, 2009). The brines have a salinity of 400 g/l TDS and a magnesium-sodium-calcium-chloride chemistry.

There are also *Lower Cambrian* and *Neoproterozoic aquifers* with a high pressure head (1200–2100 m above the top) and a salinity about 400 g/l TDS (Alekseev, 2009; Mikulenko et al., 2006). The pressure in the aquifers increases depthward and laterally toward the interior of the Tunguska basin.

The local geological and groundwater settings have been poorly studied so far. An NW fault zone dipping northeastward at 55º is known to emerge along the Marha River (Mikulenko et al., 2006), while the head of the emplacement hole is only 160 m away from the riverside. Thus, the "Kraton-3" was detonated in the immediate vicinity of the fault. The log data obtained while drilling to a depth of ~580 m is unavailable, and no drilling has been performed ever after the explosion. There is a single piece of evidence that rapid loss of drilling fluid occurred through fractured rocks between 165 and 186 m in the emplacement hole (Mikulenko et al., 2006). The lossy interval was plugged by slurry injection three times in 1978, and hydraulic pressure testing was performed. During the tests, the borehole pressure rose to 15 bar after drilling the first plug and fell to zero 4 minutes after water off. However, no more leak-off testing was applied then. We interpret this fractured interval as a local fault exposed west of the hole mouth along the river. The charge was placed in the uppermost part of Middle Cambrian clayey and marly limestone, at a depth of 577 m.

The PUNE impact on the subsurface: a summary

A wealth of experimental and theoretical data has been available by present to estimate the magnitude of the PUNE mechanic impact on surrounding rocks (Andryushin et al., 2000; Adushkin and Spivak, 2004, 2007; Sadovsky and Rodionov, 1971). The impact of the "Kraton-3" explosion was

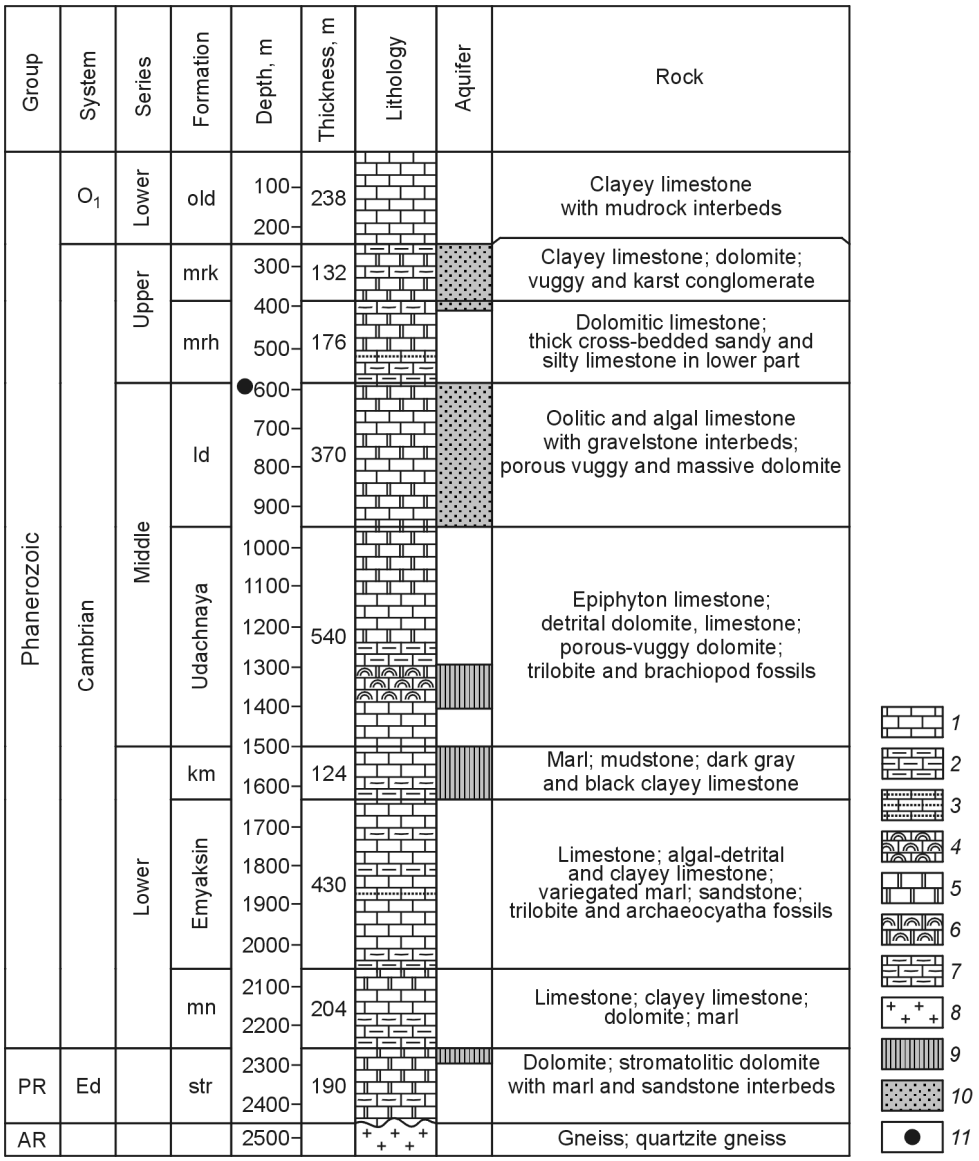

Fig. 2. Lithology synthesis (with depths of aquifers) of "Kraton-3" PUNE site, from log data, boreholes 51, 703, 95 (Alekseev, 2009). *1–4,* pure (*1*), clayey (*2*), sandy (*3*), and organic (*4*) limestones; *5*, *6,* pure (*5*) and organic (*6*) dolomite; *7,* marl; *8*, basement; *9*, Upper Proterozoic, Lower Cambrian, and Upper Cambrian II aquifers; *10*, Middle Cambrian I and Upper Cambrian aquifers; *11*, location of explosion. Abbreviations stand for the names of formations: str = Starorechenskaya, mn = Manykai, km = Kuonamka, ld = limestone-dolomite member, mrh = Markha, mrk = Markoka. Ed = Ediacaran.

assessed using empirical relationships and 1D forward modeling with *Master Professional v.1.0*. In the modeling, the laws of 1D (linear) Langrangian fluid dynamics, elastoplasticity, and detonation were applied to calculate flows attendant with sonic, shock, and detonation waves, with regard to elastoplastic deformation and tensile slabbing (Rudenko et al., 2006).

The normalized emplacement depth $H_{\text{norm}} = H/E^{1/3} = 577\ \text{m}/22^{1/3}\text{kt}^{1/3} = 206\ \text{m/kt}^{1/3}$ corresponded to a typical contained explosion. Of course, the containment failure accident caused complications to the event, but its effect was not included into calculations for the PUNE mechanic impact on the surrounding rocks at the given stage of research.

The size (volume or radius) of the containment (melt) cavity, one of main PUNE parameters, was estimated using the equation by Rodionov (Adushkin and Spivak, 2007), assuming a compression strength (bulk modulus) σ_* (Pa) exceeding the pore pressure ρgH (Pa): $\sigma_* > \rho gH$, where ρ is the rock density (g/cm^3), g = 9.8 (m/s^2), and H is the depth (m). The equation describes the dependence of the melt cavity radius on the bulk modulus σ_* and the acoustic impedance pC_p^2 of rocks:

$$R_{\text{cav}} = E^{1/3}\frac{354.6}{(\rho\, C_p^2 \sigma_{\text{compr}})^{1/9}}, \quad (1)$$

where R_{cav} is the radius of the containment cavity (m), E is the explosion yield (kt in TNT equivalent); ρ is the density of carbonate rock (g/cm^3), C_p is the sonic velocity (m/s); σ_{compr} (or σ_*) is the rock compression strength, or bulk modulus (Pa).

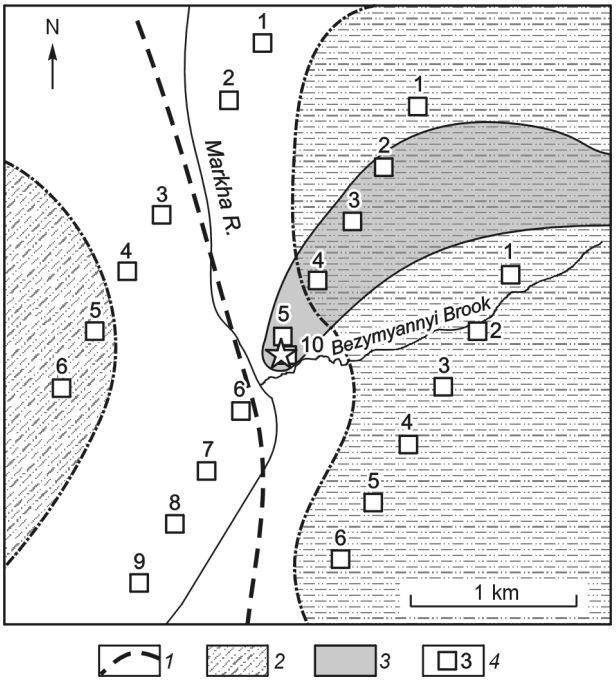

Fig. 3. Location map of TEM profiles and numbers of stations at "Kraton-3" PUNE site. *1*, inferred fault zone; *2*, extent of high-resistive permafrost (extrapolation); *3*, dry forest which died from PUNE-related radioactive pollution; *4*, measurement point and its number. Star marks the head of emplacement hole.

The containment cavity radius found according to (1) is from 29 to 32 m, at (C_p) from 5400 to 3500 m/s, and the density of carbonates assumed to be $\rho = 2.38$ g/cm^3, σ_{compr} (or σ_*) = 0.1 GPa. As the modeling showed, the cavity formed already at 30–40 ms, with a radius of 24 m, which is within ±20% relative to the value calculated with the empirical relationships.

The radius of the crushed zone R_{crush}, found as

$$R_{crush} = R_{cav}\left(\frac{\rho C_p^2}{4\sigma_*}\right)^{1/3}, \quad (2)$$

is 112–133 m. The radius of the cracked zone was found to be 168–199 m, as

$$R_{crack} = R_{crush}\left(\frac{\sigma_*}{2(\sigma_{shear} + \rho g H)}\right)^{1/2}, \quad (3)$$

where σ_{shear} is the shear or tensile strength, in this case σ_{shear} = 0.01 GPa.

This is a notional division, however, which means only that the ground experiences deformation and develops an hierarchic mosaic pattern. The distinguished deformation zones are asymmetric, the maximum strain being oriented toward the ground surface. The evolution of these zones is additionally controlled by manmade weakness domains in rocks (Adushkin and Spivak, 2007). The contribution of the containment failure event remains unclear and may be estimated by 3D modeling.

As modeling predicts, the maximum displacement reached 0.42 m and 0.17 m, while the maximum radial pressure was 0.8 GPa and 0.13 GPa at 100 m and 200 m away from the explosion epicenter, respectively.

At a certain stage after the shock there follows a rebound, when the pressure in the cavity falls and the rocks move toward it. This effect is common to explosions in hard rocks, is weak in softer ground, but does not occur in plastic ground (clay or salt), and is not taken into account in the empirical formulas. According to the modeling for the "Kraton-3" explosion, the rebound effect produced a stress containment cage (compressive forces built-up around the cavity) at 100–300 m away from the epicenter, which sealed the cracks and prevented the escape of radioactivity. At a distance of 100 m, the pressure fell suddenly at the time 30–60 ms and the rocks set into backward motion (at negative velocities) at 70–80 ms. Farther from the explosion, at 200 m, the rebound effect occurred within the time span of 55 to 90 ms. The stress containment cage collapsed at late times when the depression wave from the free surface (at hundreds of ms) produced a zone of tensile slabbing and when cave-in created a rubble chimney (at times from seconds to hours).

At the emplacement depths ~100–200 m/kt$^{1/3}$ a surface layer of ground slabbed away. According to the modeling prediction, the slabbing zone in the case of the "Kraton-3" explosion formed ~120 m below the ground (the yield-normalized depth being 206 m/kt$^{1/3}$) and had a radius of 840–1120 m on the surface (commonly R ~ 300–400 m/kt$^{1/3}$).

The expected height of the rubble chimney proceeding from the strength of limestone (6–8 times the R_{cav} according to (Adushkin and Spivak, 2007)) was ~186–249 m, but the real height is unknown. Note that this height depends on several rock parameters, as well as on the thermodynamics of the explosion products.

The very fact and the time of cave-in are controlled by the local geology and tectonics, especially, faults and fractures. In the case of "Kraton-3", there was a fractured lossy zone at 391–412 m above the charge emplacement, or 165–186 m below the surface, which we attributed to the NE fault. It remains unclear whether the rubble chimney has reached the fault zone.

TEM experiments

The permafrost and buried aquifers in the PUNE area produce prominent resistivity contrasts, the resistivity being high in dry frozen ground and low or very low in the aquifers saturated, respectively, with water or with brines, which are natural electrolytes. Therefore, the TEM method successfully applied to study the area of the "Kristall" PUNE in Yakutia (Artamonova et al., 2012; Kozhevnikov et al., 2012) was chosen for the geolectric survey at the "Kraton-3" site. TEM data were acquired in August 2008 along three parallel N–S (azimuth 26°) profiles spaced at 1 km. The longest (3300 m) central profile traversed the PUNE epicenter (Fig. 3), and two shorter profiles ran east (2000 m) and west (2400 m) of it. The acquisition was in the classical way (Vanchugov and Kozhevnikov, 1998), with a square central-loop configuration,

at 22 points. The transmitter and receiver loop sizes were 200 by 200 m and 50 by 50 m. The loop size and spacing were selected proceeding from general considerations for the lack of *a priori* information on the local resistivity structure. Sampling was at every 400 m on average, in accordance with the desired penetration depth.

The *SGS-TEM* system (Kozhevnikov and Plotnikov, 2004) included several units: a laptop and a telecommunication adapter; a synchronizer and an ampermeter; two telemeters for voltage $e(t)$ in the receiver loop and for current I in the transmitter; the 31 μs sampling rate provided high resolution. No less than 10 measurements were taken at each point as means over time series of 50 positive-negative transient pairs. The total of at least 1000 responses ensured a signal/noise ratio of 30 or better.

The discrete transient pulses were transmitted at different periods depending on the duration of the transient process. The transmitter was powered by 12–24 V acid batteries and had an amperage from 1.7 to 7.5 A. Even that low amperage was enough to measure transients at times about 100–150 ms and penetrate to 400–500 m depths due to the absence of industrial noise in the area.

The earliest time $t_{\min}$ defining the minimum penetration depth was 0.2 ms on average.

The voltage measured in the receiver loop was normalized to the transmitter current (normalized responses) and used to estimate the apparent resistivity ρ_τ, in ohm·m, as

$$\rho_\tau(t) = \left[\frac{I S_t S_r}{e(t)\, 20\pi\sqrt{\pi}}\right]^{2/3} \left(\frac{\mu_0}{t}\right)^{5/3},$$

where t is the time in seconds; S_t and S_r are, respectively, the surface areas of the transmitter and receiver loops, m^2; $e(t)$ is the voltage induced in the receiver, V; I is the transmitter current, A; $\mu_0 = 4\pi \times 10^{-7}$ H/m is the vacuum magnetic permeability (Kaufman and Morozova, 1970).

The depth-dependent behavior of the apparent (and, to a certain extent, true) resistivity shows up in its time dependences (ρ_τ curves). At the preliminary stage of studies, the depths were considered as effective values corresponding to skin depths in the frequency domain:

$$H_{ef} = k\sqrt{t\,\rho_\tau(t)}, \quad (4)$$

where H_{ef} is the effective depth, m; k is the constant; t is the time, s; and $\rho_\tau(t)$ is the apparent resistivity, ohm·m. Taking into account the previous experience of TEM data processing, H_{ef} was calculated assuming k = 500–800 (Vakhromeev and Kozhevnikov, 1988).

The transient responses were inverted within the limits of a layered-earth model using the <Unv_QQ> and <Inv_QQ> software.[1] See Fig. 4 for typical measured and computed responses (curves) at two stations: point 3 in the eastern profile and point 10 at the PUNE epicenter, central profile (Fig. 4*a*), and two variants of the corresponding models (Fig. 4*b*), with the rms errors 4% and 5%, respectively, in variant 1 (Fig. 4*b*).

Proceeding from the local geology knowledge (Alekseev, 2009; Mikulenko et al., 2006), a thin layer with very low resistivity (C1, Fig. 4*c*) was distinguished within the top of the thick layer L3. The latter was identified as the Upper Cambrian Markoka and Markha limestone and dolomite and C1 was tied to an Upper Cambrian low-water aquifer with brines. Incorporating the C1 conductor into the model reduced the rms misfit between the field and computed data by a factor of 1.5.

Results and discussion

The apparent resistivity curves measured at 22 points of the three profiles (Fig. 5) have features of both similarity and difference. Those from the *eastern profile* laid on the watershed in the right side of the Markha (Fig. 3) show a uniform pattern (Fig. 5*a*). They diverge slightly at early times (ρ_τ are very high at t < 0.2–0.3 ms) but are identical at late times. The curves, almost coinciding about 10 ms, reveal a conductor between 10 and 30 ms and another one, with a still lower resistivity, at t ~ 30–100 ms. The curves become steeper at t > 100 ms and thus hint to a conductive section bottom. We write "hint" because the signals at these times are low and the interpretation may bear significant uncertainty.

The resistivity-depth curves for different times (Fig. 6) are more closely spaced after 10 ms (Fig. 6*a*), this being a boundary between more resistive rocks above and more conductive rocks below. Generally, the curves are smooth all along the eastern profile and image a laterally uniform geoelectric pattern. It corresponds to the model ($\rho_1 > \rho_2 > \rho_3 > \rho_4$, where ρ_1, ρ_2, ρ_3 are the resistivities of the layers L1, L2, L3, from top to bottom, and ρ_4 is the resistivity of the lowermost layer (section base).

The responses from the *central profile* fall into two groups (Fig. 5*b*). Those of points Nos. 1–4 located on the watershed in the northern flank are similar to the ρ_τ curves of the eastern profile and to one another, but differ from the other curves of the central profile. Namely, the resistivities are high at early times (t < 0.2–0.3 ms) though are notably lower than ρ_τ measured in the eastern profile. The resistivity at $t \le 10$ ms decreases progressively from point 1 to 4, i.e., from the watershed to the river.

The closer spacing of ρ_τ curves likewise marks a boundary between more resistive rocks above and more conductive rocks below at times about 10 ms, which corresponds to the effective depths about 200 m. The tails of the curves at t > 100 ms are still flat, unlike the steeply falling ones in the eastern profile, i.e., the resistivity of the lowermost layer is slightly higher than in the east.

The curves from points 5 to 10 of the central profile are dissimilar to one another but generally show much lower resistivity values. Prominent lows are measured at two neighbor points (5 and 10) within the earliest times $t \le 0.25$ ms. The general trend at the early times, except the anomalously

[1] Designed by E.Yu. Antonov, IPGG, Novosibirsk.

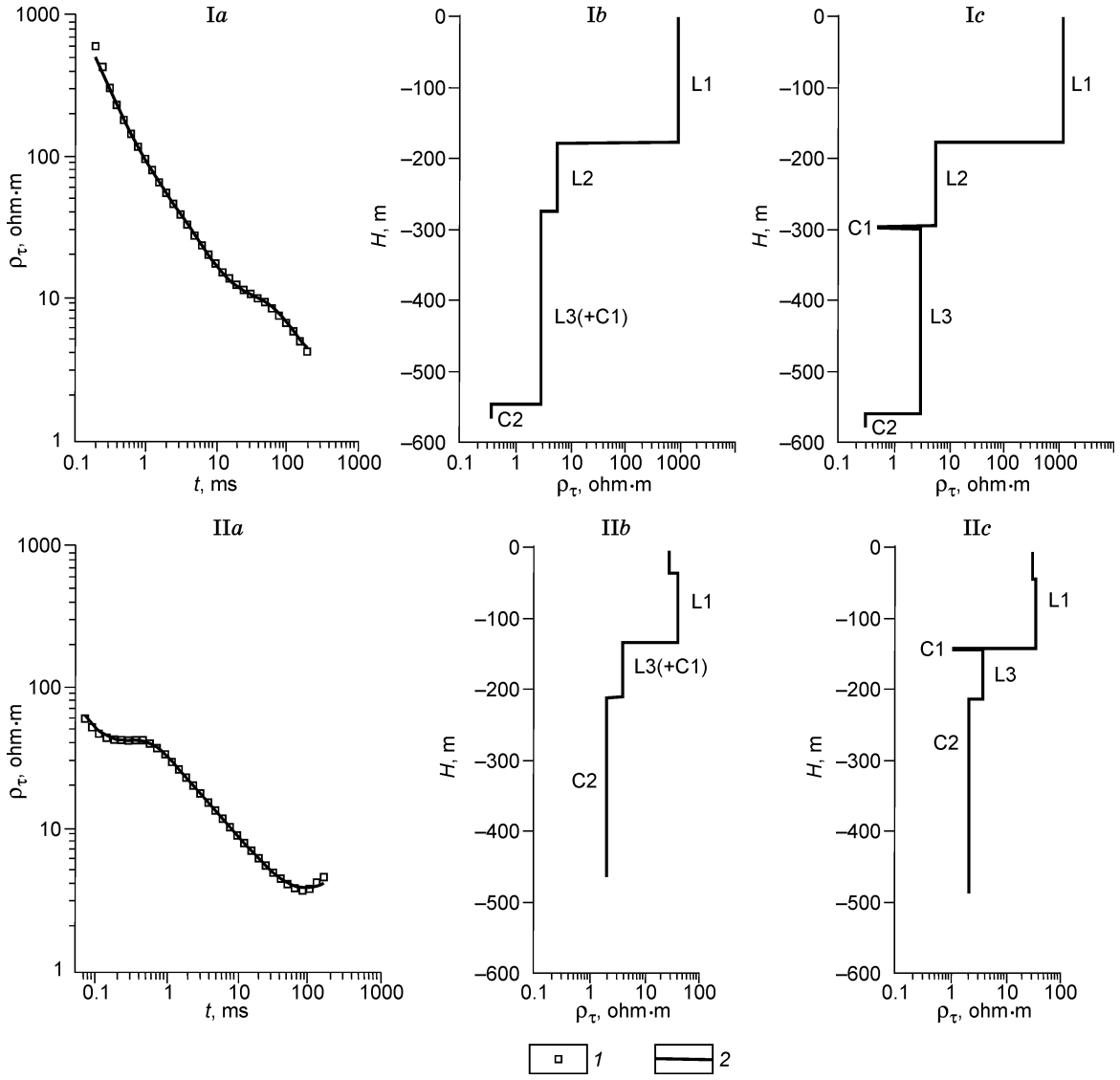

Fig. 4. Measured (*1*) and computed (*2*) apparent resistivity curves (ρ_τ) (*a*) and respective 1D models (*b* = variant 1; *c* = variant 2). I, 1 km east of PUNE epicenter (point 3, eastern profile); II, at PUNE epicenter (point 10, central profile). Abbreviated names of resistivity layers are as in Table 1.

low ρ_τ at points 5 and 10, is a decrease from north to south, which is evident in the depth curves (Fig. 6*b*). At point 9, ρ_τ drops between 0.15 and 0.6 ms (Fig. 5*b*). The ρ_τ curves become closer at later times ($t \geq 4$ ms), i.e., the resistivity anomaly narrows down with depth, except for point 10, where the resistivity keeps decreasing, though the curve turns upward in the tail and approaches the other curves. The central part of the profile (near the explosion) generally has very low ρ_τ, but the variability of the ρ_τ curves is evidence of a complex lateral structure of the subsurface.

The resistivity curves of the *western profile* (Fig. 5*c*) are similar to one another, except those measured at points 3 and 4 in the left bank of the Markha. The early-time ρ_τ at these points are notably lower than in the other curves. At the times $t < 0.2$–0.3 ms, the apparent resistivities are 10 times as low as in the eastern profile. Furthermore, the ρ_τ curves have ascending branches at late times ($t > 100$ ms), indicating a higher resistivity at the section base relative to that along the eastern profile. The late-time resistivity high of ρ_τ = 1960 ohm·m measured at point 4 most likely records a 2D or 3D local feature. The anomalous (heterogeneous) subsurface structure at this point is additionally indicated by lower levels and closer spacing of curves in Fig. 6*c*.

Apart from details, the resistivity pattern of the PUNE site (Fig. 4*b*) fits a *QQ* four-layer earth model with a highly conductive layer at the base (ρ_4): $\rho_1 > \rho_2 > \rho_3 > \rho_4$, within the TEM penetrated depths of 500 m below the surface or 200 m below the sealevel (down to ~640 m and 300 m, respectively, at some points). The apparent resistivity of the layers decreases (and the conductivity increases) with depth, from early to late times, though the resistivity values and their ranges are different in each layer.

We selected, by means of inversion, the best-fit four-layer models for each response, with certain resistivity values and

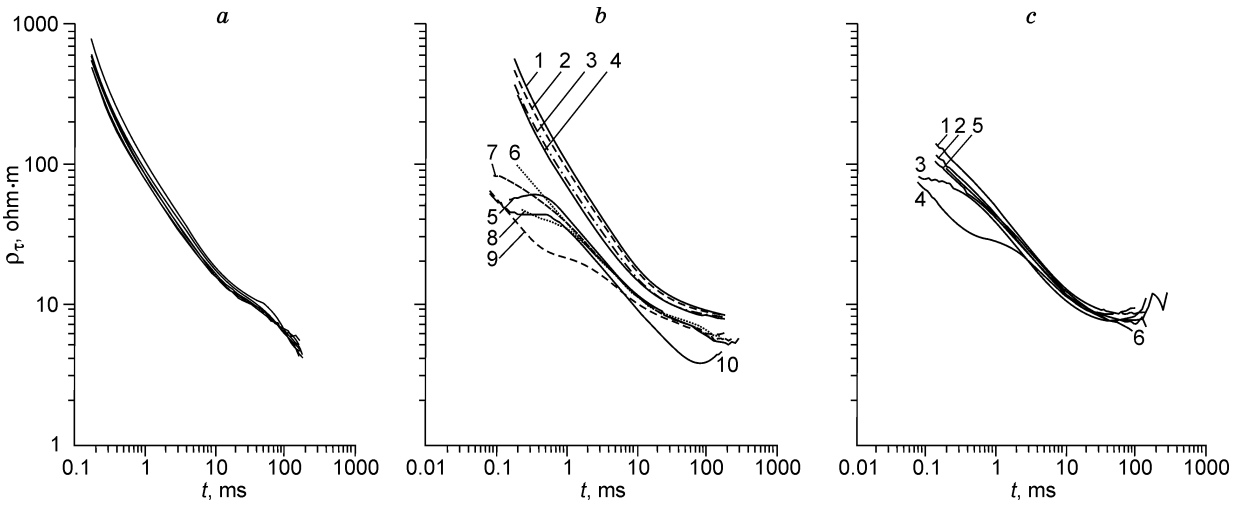

Fig. 5. Apparent resistivities (ρ_τ) measured along eastern (*a*), central (*b*), and western (*c*) profiles. Numerals 1–10 are numbers of measurement points.

layer thicknesses. The four layers are especially well evident in the eastern profile, where the resistivity is the highest (1100–1200 ohm·m) in the upper layer and decreases rapidly with depth. Namely, it drops to 5.6–6.9 ohm·m, or hundreds of times, on transition between ρ_1 and ρ_2, i.e., the contrast is very large. The resistivities are ρ_3 ~ 2.4–4.1 ohm·m in layer 3 and ρ_4 = 0.3 to 0.7 ohm·m in the lowermost layer of the model. Therefore, the more correct relationship will be $\rho_1 \gg \rho_2 > \rho_3 > \rho_4$, which fits all three profiles.

The obtained resistivity patterns are interpreted below in terms of geology. The uppermost resistive layer L1 (ρ_1), prominent at all stations, likely corresponds to the permafrost. Note that its base (including unfrozen lenses) is almost flat, i.e., the layer is rather uniform (Fig. 7).

The data for L1 are either within 100 ohm·m or largely above this value, mainly tending at $\rho_1 = 10^3$ ohm·m. What may be the reason for such a large resistivity difference within a single carbonate layer? The only plausible explanation may be that the less resistive rocks ($\rho_1 < 100$ ohm·m) are unfrozen while those with $\rho_1 \gg 100$ ohm·m are frozen. The difference in temperature and water contents of sediments in L1 defines the variations from the highly resistive strongly frozen ground along the eastern profile to unfrozen rocks in the western profile and in the southern flank of the central profile.

The permafrost in L1 is thick (160–200 m) and the resistivity is high (680 to 1200 ohm·m) on watersheds or on elevated slopes along the right side of the Markha Valley, in the eastern profile and in the northern flank of the central profile. Toward the river, the permafrost thins down from 200 to 150 m, both in the eastern profile and in the north of the central one, and the resistivity decreases from 800 to 600 ohm·m between points 1 and 4 in the central profile (Table 1; Figs. 5–7). Highly resistive permafrost in L1 (to 1410 ohm·m) occurs also at high elevations on the Markha left bank, in the southern flank of the western profile.

Thus, permafrost in watershed areas is well preserved, with large thicknesses and high resistivities. This allowed us to contour zones of high-resistivity permafrost by extrapolation of TEM data (Fig. 3). The layer L1 becomes thinner (~80–110 m) in hypsometrically lower parts of the valley sides, and the resistivity changes both in lateral and vertical dimensions, from 30 to 100 ohm·m (Table 1; Fig. 7). The lower portion of L1 is less resistive, from 20 to 50 ohm·m, and is apparently unfrozen and more or less wet. Warmer rock temperatures and higher water contents may result from joint action of natural (water and local tectonics) and man-caused (explosion) agents that maintain the formation of taliks (unfrozen zones).

More specifically, (1) water of rivers and lakes is known to warm up the permafrost and produce lenses of unfrozen ground underneath: there is commonly no permafrost under large rivers (Klimovsky and Gotovtsev, 1994); (2) the fault emerging along the river (Mikulenko et al., 2006) can conduit natural heat from the Earth's interior; (3) the mechanic and thermal impacts of the explosion may have enhanced the natural effects: the shock waves opened the fault and deformed the surrounding rocks thus creating paths for material and heat transport from the explosion to the ground surface.

The transition to ρ_2 (10.0–17.7 ohm·m) from the "warm" rocks of L1 is not as sharp as within the watershed permafrost. The lower resistivity of L2 (Fig. 7), which we call a transitional layer, may result from its warmer temperature and higher water contents relative to L1. Furthermore, a higher overburden pressure and a lower porosity increase the conductivity of dry rocks. The resistivity of rocks in L2 (ρ_2) is more uniform than in L1: it is 5.6–6.4 ohm·m in the eastern profile (see above), 7–10 ohm·m in the central profile, and mostly from 8 to 18 ohm·m in the western profile. On the background of generally low resistivities in L2, there is a weak second-order increasing trend from the watershed on the Markha right bank toward the river and the flatter left bank. This may be due to larger porosity in the fault zone along the river. As an additional support to this inference, we note that the increasing trend in L2 correlates inversely with the decreasing trend in L1.

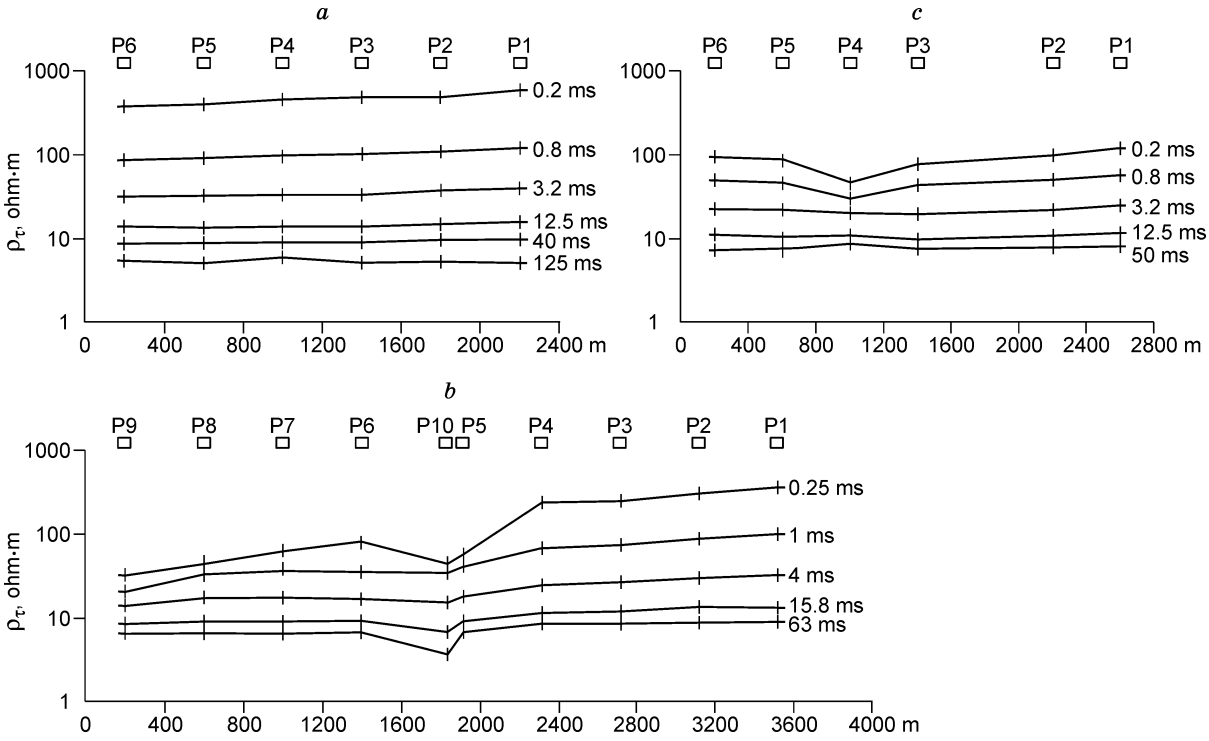

Fig. 6. Apparent resistivity-depth profiles (ρ_τ) at different times measured along eastern (*a*), central (*b*), and western (*c*) profiles. Numerals P1–P10 are measurement points.

The thickness of L2 within the eastern profile is more uniform (118–130 m, its bottom lying at 30 to 60 m asl) than in the central one. The layer (Fig. 7, Table 1) is locally mute because of highly conductive brines rising from the underlying aquifer (see below). It thins down from 100 to 50 m in the N–S direction within the western profile as its bottom shallows down being generally more highly elevated than along the eastern profile (80–140 m asl). The elevation of the L2 top along the two profiles is uniform, about 200 m asl. The thickness of the layer depends mainly on the level of underground brines corresponding to the layer L3 with very low ρ_3. The layer L2 corresponds to Lower Ordovician and Upper Cambrian dry limestone and dolomite.

The layer L3 beneath L2, which we identify as wet dense carbonates of the Upper Cambrian Markoka and Markha formations, is 200–350 m thick, and ρ_3 in it is as low as 2.4 to 4.9 ohm·m, indicating high contents of saline water. The same depth interval, near the top, comprises a subpermafrost thin undersaturated Upper Cambrian aquifer with saline waters from 30 to 250 g/l TDS (90 g/l on average). Chloride waters of such a salinity have resistivities of the order of 0.1–0.5 ohm·m. Proceeding from this evidence of the groundwater setting (Alekseev, 2009; Klimovsky and Gotovtsev, 1994; Mikulenko et al., 2006), we have distinguished, by fitting, a thin conductor ρ_{3-1} of 0.4–1.6 ohm·m within the upper part of L3. Incorporation of this layer (C1) improved the inversion quality as the rms error reduced by a factor of ~1.5: from 4–5 to 3.0–2.5%, though its contribution to the total conductivity is minor (5–7%). The results of <Unv_QQ> and <Inv_QQ> inversion for the five-layer assumption are given in Table 1.

The top of C1 has elevations from 20 to 80 m asl; its inferred average thickness of 2–3 m is close to the measured thickness of the Upper Cambrian aquifer in the eastern periphery of the Tunguska basin (Alekseev, 2009). The layer C1 is most likely discontinuous on strike (shown by hatching in Fig. 7) and corresponds to fractured and porous vuggy dolomite and limestone of the Upper Cambrian Markoka Formation.

Another resistivity sublayer within the lower L3, ρ_{3-2} (no special name), is from 3.8 to 5.8 ohm·m, or about that of the other layer part (Fig. 4*b*, *c*; Table 1). The resistivity values from points 9 and 1 (11.7 ohm·m and 65.0 ohm·m, respectively) of the central profile require an additional check.

The layer L3, 200–250 m of average thickness most likely consists of wet dense Upper Cambrian carbonates of the Markha Formation. Along the eastern profile, L3 lies over a still more conductive layer (0.3–0.8 ohm·m), hardly discernible at late times where the transient responses are comparable with noise, this deteriorating the interpretation quality. We interpret it as the Middle Cambrian aquifer I and distinguish as layer C2. The top of the C2 conductor (ρ_4 = 0.2–1.9 ohm·m) is as deep as 550–640 m below the surface (200 to 300 m below sealevel) in the eastern profile but is shallower (150 to 50 m bsl) in the western profile. A similar conductor, with the same low resistivity and at the same depths, was detected at the site of the "Kristall" PUNE (Artamonova et al., 2012). There is only one plausible explanation for the very low resistivity (~1 ohm·m) of rocks at the depth about 500 m: highly saline pore water, with a salinity known to average about 300 g/l.

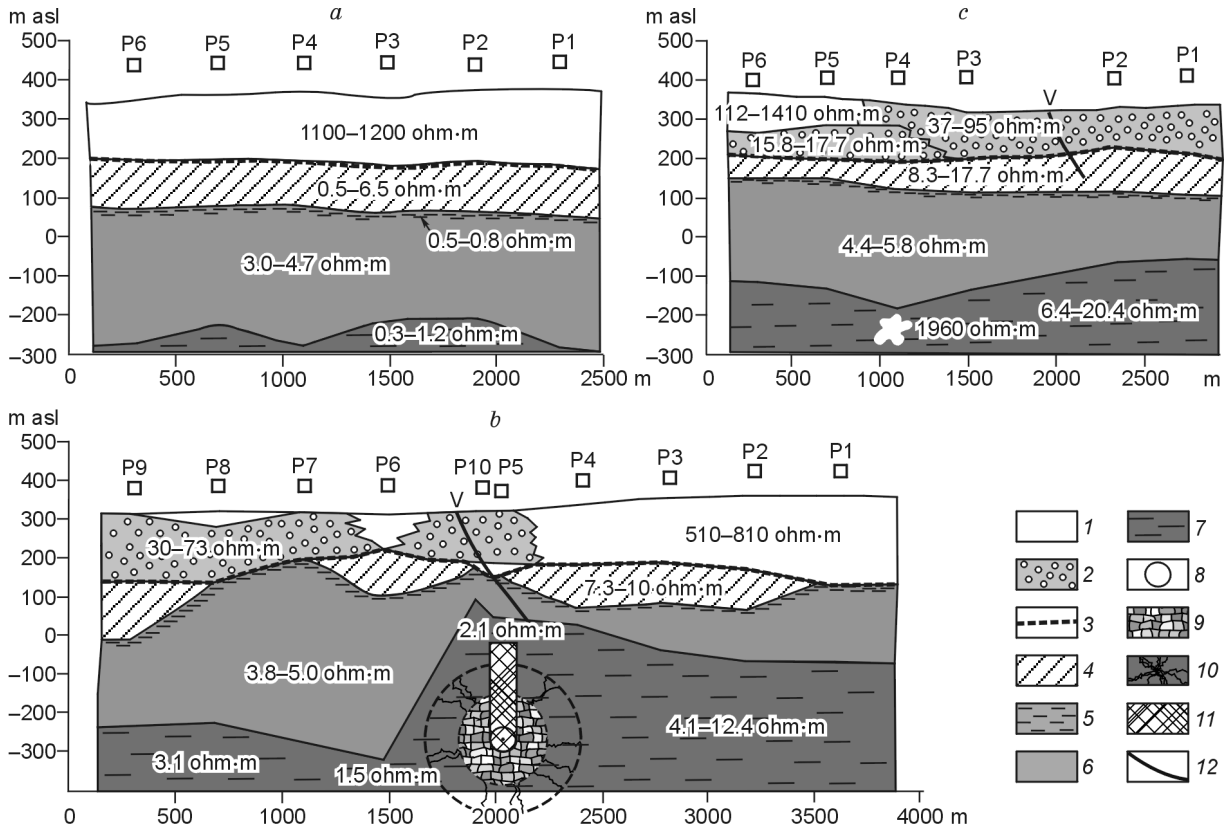

Fig. 7. A model of permafrost and groundwater setting at "Kraton-3" PUNE site along eastern (*a*), central (*b*), and western (*c*) profiles. *1*, permafrost; *2*, degrading permafrost with zones of warmer and wetter (unfrozen?) rocks; *3*, permafrost base; *4*, subpermafrost dry (frost-bound) Lower Ordovician limestone and dolomite; *4*, thin (to 2–3 m) Upper Cambrian aquifer with brines; *5*, Upper Cambrian wet (frost-bound) rocks; *7*, Middle Cambrian aquifer with brines (white spot marks measured resistivity high); *8–11*, zones of PUNE mechanic impact, to the vertical scale of the model: containment cavity (*8*), crushed zone (*9*), cracked zone, radiated cracks (*10*), rubble chimney (*11*); *12*, inferred fault plane. P1 through P10 are measurement points and their numbers; V marks Markha riverbed.

The resistivity of C2 is slightly higher within the central and western profiles, as the tails of the ρ_τ curves often form ascending branches instead of falling steeply down. Rocks in the lowermost part of the section at point 4 of the western profile have an unusually high resistivity of $\rho_1 = 1900$ ohm·m, most likely due to a 2D or 3D local feature (see above).

The resistivity pattern along the central profile over the explosion is more complicated than elsewhere: a zone of low resistivity appears at stations 5 and 10 above the cavity till the surface. The TEM penetration depth being shallower than the explosion, there is nothing else to suggest but a fractured permeable zone saturated with saline waters from C2. The TEM data reveal an abrupt ~300 m rise of pressurized saline groundwater vertically from the containment cavity, the lateral extent of the anomaly being ~400 m. The brines from the Middle Cambrian aquifer I apparently rose, under confining pressure, along the permeable zone of the rubble chimney. The calculated height of the chimney, 186–249 m, is about the same order as the vertical size of the groundwater anomaly. The presence of a fault at 391–412 m above the explosion, along with the containment failure and the related additional gas-dynamic driving force of the explosion, may be responsible for an actual size of the rubble chimney larger than it was expected. The explosion itself must have opened the fault, this hypothesis being consistent with reported radioactive pollution of surface water where manmade radionuclides come from the containment cavity (Artamonova, 2012). Retrospective 3D modeling of the explosion and a higher-density TEM survey will provide more details of the subsurface structure at the "Kraton-3" site.

Conclusions

The reported TEM data allowed us, for the first time, to image and discuss the resistivity pattern at the site of the "Kraton-3" contained nuclear explosion to a depth of ~500 m below the surface or 200 m below the sealevel (~640 m and 300 m, respectively, at some stations). The obtained resistivity models were interpreted proceeding from the available knowledge of local stratigraphy, lithology, permafrost, and groundwater settings.

The background subsurface structure at the PUNE site comprises several plane layers. The highly resistive uppermost layer, with quite a uniform thickness of ~150–200 m, consists of perennially frozen ice-rich rocks. The coldest dry rocks, with resistivity to 1200 ohm·m, occur on watersheds in the Markha right side. The permafrost is degrading in the

Table 1. Thicknesses and resistivities of layers distinguished in TEM data from "Kraton-3" PUNE site

Point number	*H*	Longitude, deg	Latitude, deg	L1 (ρ_1)	L2 (ρ_2)	C1 (ρ3–1)	L3(ρ3–2)	C2 (ρ4)
		E	N					
Eastern Profile								
P1	376.2	112.3622	65.9307	199* (1100)	123 (6.3)	8 (0.8)	323 (4.7)	(1.2)
P2	370.1	112.3583	65.9275	182.6 (1120)	119 (6.4)	4.4 (0.7)	266 (3.6)	(0.6)
P3	354.6	112.3543	65.9243	176 (1200)	118 (5.6)	3 (0.5)	261 (3.0)	(0.3)
P4	367.2	112.3504	65.9211	172.6 (1140)	124.5 (6.5)	3 (0.6)	340 (3.6)	(0.8)
P5	361.2	112.3464	65.9179	164 (1150)	121 (6.3)	2.4 (0.6)	294 (3.5)	(0.8)
P6	355.3	112.3425	65.9147	162 (1150)	131 (6.4)	2.3 (0.6)	332 (4.0)	(1.2)
Central Profile								
P1	363.4	112.3273	65.9421	146.8 (510) 70.8 (400)	–	2.3 (0.5)	28.6 (65.0)	(4.9)
P2	360.0	112.3234	65.9389	175 (810)	107.9 (8)	2.9 (0.7)	139.6 (4.7)	(7.5)
P3	355.7	112.3196	65.9357	158.1 (730)	105.2 (7.7)	2.2 (0.6)	120.7 (4.5)	(6.6)
P4	340.3	112.3157	65.9325	148.8 (680)	114.5 (7.3)	2.1 (0.6)	33.5 (3.8)	(6.1)
P5	318.5	112.3118	65.9293	125.1 (45.6) 24.1 (630)	–	2.2 (1.1)	110.3 (5.0)	(4.1)
P10	317.8	112.3099	65.9276	39.3 (30.0) 98.7 (35.5)	–	2.2 (1.1)	69.1 (3.8)	278.6 (2.1)
P6	313.0	112.3080	65.9260	79.7 (780)	120.4 (10)	2.1 (0.4)	434.2 (4.6)	(1.5)
P7	315.6	112.3041	65.9228	5.2 (73.0) 100.4 (50.0)	–	2.0 (1.6)	51.0 (19.8)	(4.4)
P8	322.6	112.3002	65.9196	25.6 (140) 144.7 (22.6)	–	2.2 (0.9)	369.0 (4.0)	(3.1)
P9	323.0	112.2964	65.9164	75.1 (75.3) 100 (33.7)	143.6 (33.7 ?)	2.0 (0.5)	(11.7)	–
Western Profile								
P1	332.9	112.3273	65.9421	122.8 (88)	92.4 (9.7)	2.0 (0.5)	165.7 (4.9)	(8.7)
P2	321.5	112.3234	65.9389	97.5 (95)	96.2 (12.5)	2.0 (0.5)	184.2 (4.8)	(6.6)
P3	313.4	112.3157	65.9325	110.9 (53)	82.1 (8.3)	1.9 (0.4)	243.0 (4.7)	(20.4)
P4	336.3	112.3118	65.9293	41.4 (37.0) 105 (17.7)	64.0 (17.7)	3.9 (0.4)	302.0 (5.8)	(1960)
P5	351.2	112.3079	65.9260	60.8 (1410) 80 (17.4)	43.0 (17.4)	2.0 (0.6)	295.4 (4.6)	(16.0)
P6	358.9	112.3040	65.9228	81.9 (112) 58 (15.8)	53.9 (15.8)	1.3 (0.5)	267.6 (4.4)	(6.4)

Note. *H* is the asl elevation, in m. Geological interpretation of resistivity layers: L1 = perennially frozen Lower Ordovician sediments with unfrozen zones; L2 = subpermafrost dry Lower Ordovician sediments; C1 = Upper Cambrian aquifer with brines; L3 = Upper Cambrian wet (frost-bound) rocks; C2 = Middle Cambrian aquifer I with brines. Numerals in parentheses are resistivities in ohm·m. * Thickness of resistivity layer, in m.

hypsometrically lower areas, where a fault runs along the river, exactly where the PUNE epicenter is located. The degradation of permafrost is evident in low resistivities (30–100 ohm·m or locally to 20 ohm·m) and their uneven vertical and lateral distribution. The taliks (unfrozen zones) we detected may have natural causes associated with the warming effect of the river and flow of deep heat through the faulted rocks. However, we cannot rule out and rather suggest that the mechanic and thermal impacts of the explosion have been an additional, and a critical, trigger for permafrost degradation along the fault. The PUNE-induced deformation can have reactivated the fault and opened heat and mass conduits to the ground surface.

Conductive layers (0.4–1.1 ohm·m) in our model correspond to aquifers, namely, the Upper Cambrian and Middle Cambrian I aquifers with brines.

TEM data indicate an abrupt ~300 m rise of pressurized saline water (the Middle Cambrian I brines) from the containment cavity, most likely along the rubble chimney. The lateral extent of this local groundwater anomaly is ~400 m. Paths for the transport of heat and material (including radionuclides) must exist in the system "UNE containment cavity–rubble chimney–fractured fault zone–ground surface". This inference is supported by high concentrations of manmade radionuclides, without dilution in swampy pools, rills flowing into the

Markha, and in the river itself, to a distance of 3 km from the PUNE epicenter (Artamonova, 2012).

The study was carried out as part of the Nature Protection Program of the Sakha Republic (Yakutia), Government contract No. 43 (76-08), with support from the Department of Radiation Safety of the Ministry of Nature Protection of the Sakha Republic (Yakutia).

References

Adushkin, V.V., Spivak, A.A., 2004. Effects of underground nuclear explosions on rock properties. Fizika Goreniya i Vzryva 40 (6), 15–24.

Adushkin, V.V., Spivak, A.A., 2007. Underground Explosions [in Russian]. Nauka, Moscow.

Alekseev, S.V., 2009. Permafrost-Groundwater Systems of the Yakutian Diamond Province [in Russian]. Akademicheskoe Izd. "Geo", Novosibirsk.

Andryushin, I.A., Ilkaev, R.I., Mikhailov, V.N., Chernyshev, A.K., 2000. Nuclear Tests in the USSR [in Russian]. RFNC-VNIIEF, Sarov, Vol. 4.

Artamonova, S.Yu., 2012. Radioactive setting at the site of the "Kraton-3" underground nuclear explosion of 1978 (Northwestern Yakutia). Khimiya v Interesakh Ustoichivogo Razvitiya 20 (2), 143–155.

Artamonova, S.Yu., Bondareva, L.G., Antonov, E.Yu., Kozhevnikov, N.O., 2012. Geoecological model of "Kristall" peaceful underground nuclear explosion area (Yakutia). Geoekologiya. Inzhenernaya Geologiya. Gidrogeologiya. Geokriologiya, No. 2, 143–158.

Kaufman, A.A., Morozova, G.M., 1970. Transient Electromagnetic Surveys: Theoretical Background [in Russian]. Nauka, Novosibirsk.

Klimovsky, I.V., Gotovtsev, S.P., 1994. The Permafrost Zone of the Yakutian Diamond Province [in Russian]. Nauka, Novosibirsk.

Kozhevnikov, N.O., Plotnikov, A.E., 2004. Estimating the potentialities of the TEM method for studying shallow ground. Geofizika, No. 6, 33–38.

Kozhevnikov, N.O., Antonov, E.Yu., Artamonova, S.Yu., Plotnikov, A.E., 2012. The geoelectric structure at the site of "Crystal" underground nuclear explosion (Western Yakutia), from TEM data. Russian Geology and Geophysics (Geologya i Geofizika) 53 (2), 185–193 (237–249).

Mikulenko, K.I., Chomchoev, A.I., Gotovtsev, S.P., 2006. Underground Nuclear Explosions in the Territory of Sakha Republic (Yakutia): Geological and Geophysical Setting and Consequences [in Russian]. Izd. YaNTs SO RAN, Yakutsk.

Rudenko, V.V., Shaburova, M.V., Chekhunov, E.V., 2006. The *MASTER* software, for education and research in continuum physics, in: Software for Science. Proc. Region. Conf., 2–3 February 2006, St. Petersburg [in Russian]. Technological University, St. Petersburg, pp. 121–124.

Sadovsky, M.A., V.N. Rodionov (Eds.), 1971. The Mechanic Impact of Underground Explosion [in Russian]. Nedra, Moscow.

Vakhromeev, G.S., Kozhevnikov, N.O., 1988. TEM Methods for Mineral Exploration [in Russian]. Irkutsk University Press, Irkutsk.

Vanchugov, V.A., Kozhevnikov, N.O., 1998. Methods and results of TEM surveys for the resistivity structure of the Nakyn kimberlite field (Western Yakutia), in: Uchitel, M.S. (Ed.), Geology, Prospecting, and Exploration of Mineral Deposits. Collection of Papers [in Russian]. Irkutsk Technological University, Irkutsk, pp. 164–176 (Transactions, Irkutsk Technological University, Issue 22).

Editorial responsibility: M.I. Epov